

## **Zr<sup>4+</sup>-based metal organic gel as a fluorescent "Turn on-off" sensing platform for selective detection and adsorption of Cr (VI)**

Wen-sheng Liu,<sup>a</sup> Yong Yang,<sup>a</sup> Qian-kun Zhong,<sup>a</sup> Zhi-peng Xu,<sup>a</sup> Ju-zhou Zhang,<sup>b</sup> Bang-ben Yao,<sup>c</sup> Xiao Lian\*,<sup>a</sup> and He-lin Niu\*,<sup>a</sup>

<sup>a</sup> *AnHui Province Key Laboratory of Chemistry for Inorganic/Organic Hybrid Functionalized Materials, Institutes of Physical Science and Information Technology, Key Laboratory of Structure and Functional Regulation of Hybrid Materials of Ministry of Education, Department of Chemistry, Anhui University, Hefei 230601, PR China.*

<sup>b</sup> *China National Center for Quality Supervision and Test of Agricultural-Avocation Processed Food, Anhui Provincial Institute for Food and Drug Test, Hefei, 230051, P.R. China.*

<sup>c</sup> *Anhui Province Institute of Product Quality Supervision & Inspection, Hefei 230051, P. R. China.*

*Corresponding Author: E-mail: niuhelin@ahu.edu.cn, lianx@ahu.edu.cn.*

*† Wen-sheng Liu and Yong Yang completed the same workload.*

## **Water stability of Zr-MOG-2**

Varies of aqueous solution with a wide range of pH (1-12) is formulated with sulfuric acid ( $\text{H}_2\text{SO}_4$ ) and sodium hydroxide ( $\text{NaOH}$ ) for water stability testing. As evidenced by the powder XRD of Fig. S1, **Zr-MOG-2** remained intact after soaking for 24 h in an aqueous solution of pH=1-10. The XRD diffraction peak of the **Zr-MOG-2** xerogel changed significantly after the pH > 10. This may be due to the fact that the strong alkaline atmosphere changed the charged properties of the ARG and affected the interaction between the central metal ion and the ligand (The isoelectric point of arginine is pH=10.76). In addition, the fluorescence emission spectrum of the **Zr-MOG-2** did not change significantly after treatment with different pH atmospheres (Fig. S2). It implies that the **Zr-MOG-2** has stable photoluminescence properties in a wide pH range. The LMCT effect is not destroyed by the strong alkaline environment. Therefore, **Zr-MOG-2** has excellent photoluminescence stability in water, making it a promising new sensing material in water-related systems.

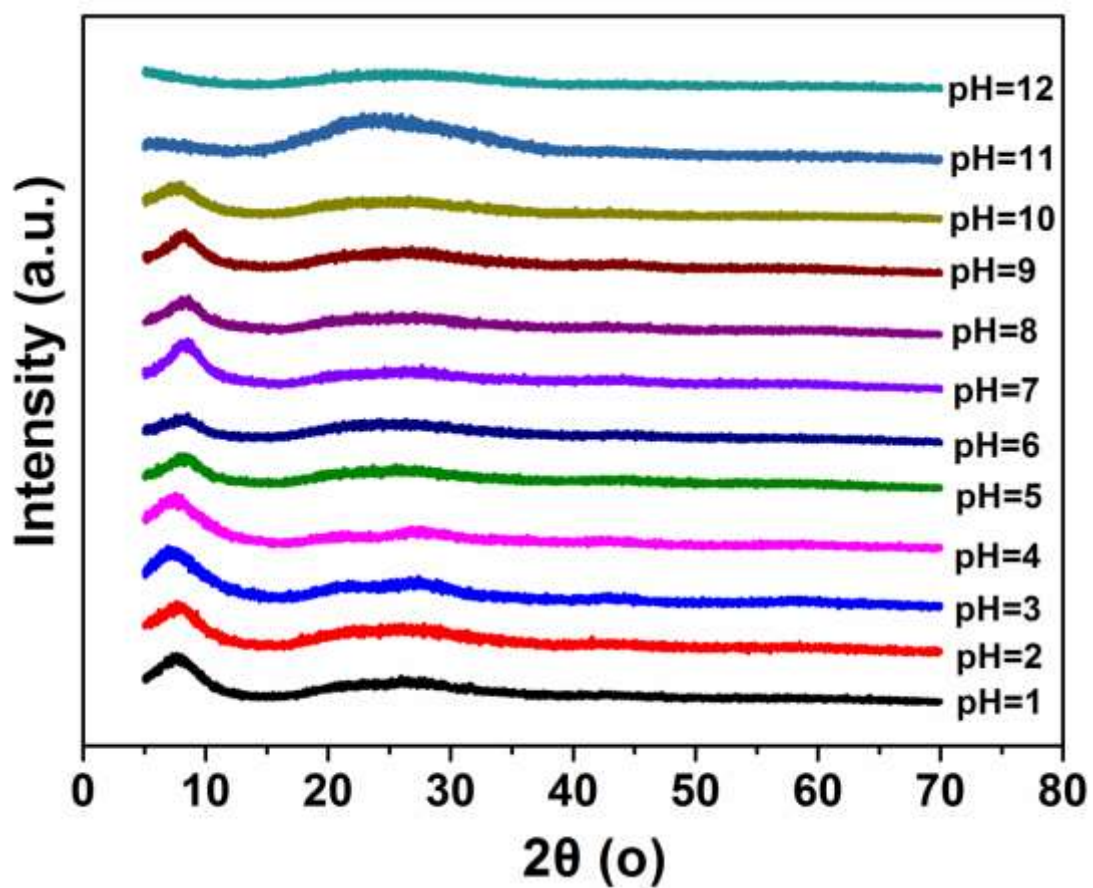


Fig. S1 The PXRD pattern of **Zr-MOG-2** xerogel after being immersed in aqueous solutions of different pH for 24 h.

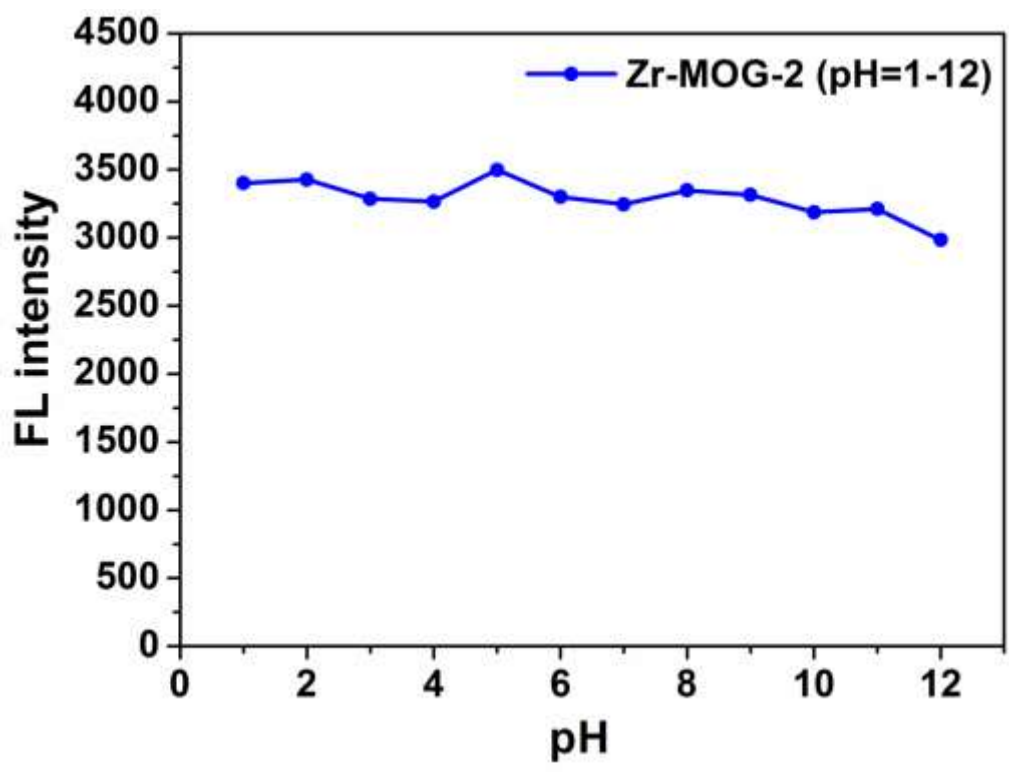


Fig. S2 Fluorescence intensity of **Zr-MOG-2** xerogel in different pH aqueous solution.

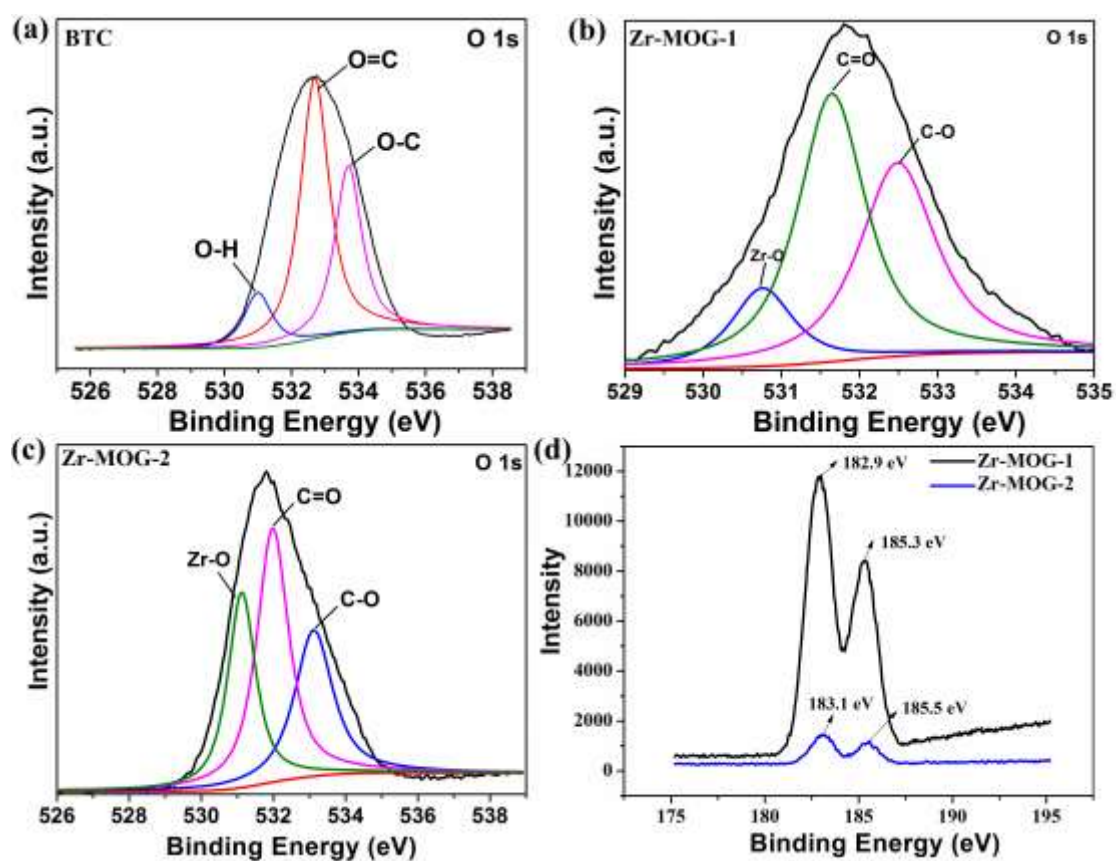


Fig. S3 O1s XPS of BTC (a), Zr-MOG-1 (b) and Zr-MOG-2 (c). Zr3d XPS of Zr-MOG-1 and Zr-MOG-2 (d).

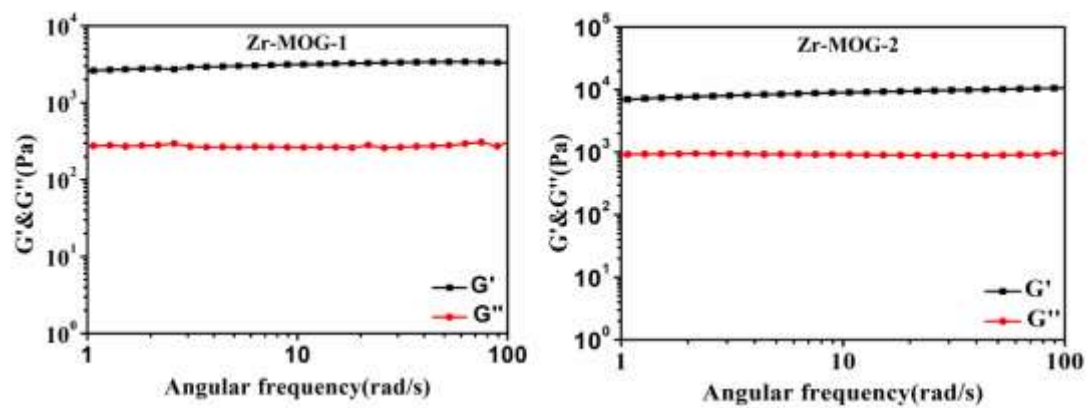


Fig. S4 Rheological curves of Zr-MOG-1 and Zr-MOG-2.

### Swelling kinetics measurement and analysis

Accurately weigh a certain amount of xerogel sample and place it in deionized water. The water on the surface of the gel is removed at regular intervals. The mass of the gel after removing the surface moisture is recorded until the recorded mass is constant, indicating that the swelling has reached equilibrium. The result is shown in Fig. S5. The swelling degree ( $Q_t$ ) of the gel is calculated according to the following formula:

$$Q_t = \frac{m_t - m_d}{m_d} \quad S1$$

Where  $m_t$  is the weight of the gel when the time period is  $t$  or the mass is constant,  $m_d$  is the quality of xerogel without swelling.

The swelling degree of **Zr-MOG-1** and **Zr-MOG-2** at equilibrium is estimated to be 1.814 and 2.106, respectively. The results indicate that the introduction of ARG increases the hydrophilicity of the gel so that **Zr-MOG-2** xerogel can absorb water and swell more quickly.

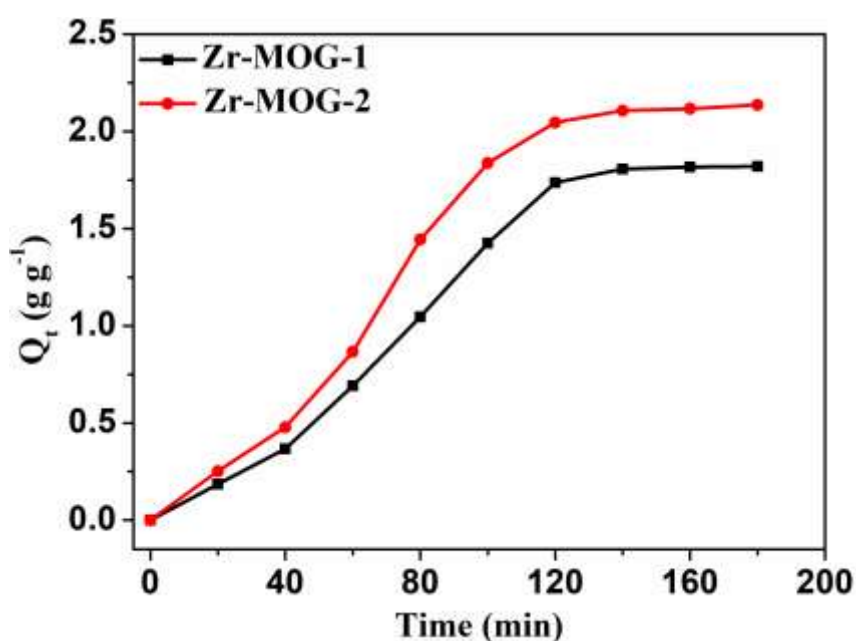


Fig. S5 Swelling behavior of **Zr-MOG-1** and **Zr-MOG-2** in aqueous solution at 25 °C.

## Determine and analysis the moisture content of the gel

The **Zr-MOG-1** and **Zr-MOG-2** hydrogel samples were taken out and the surface moisture was removed. Weigh its quality. The sample is then placed in the freeze dryer and freeze-dried until constant weight. The mass of the xerogel obtained is weighed to estimate the moisture content. The moisture content (mass fraction) in the sample is calculated by the following formula:

$$\mathbf{W} = \frac{m-m_0}{m} \times \mathbf{100\%} \quad \mathbf{S2}$$

Where  $m$  is the mass of the hydrogel sample,  $m_0$  is the mass of the xerogel after the sample is lyophilized. The moisture content of **Zr-MOG-1** and **Zr-MOG-2** at equilibrium is estimated to be 23.78% and 34.39%, respectively. The result may be attributed to the factor that the introduction of the ligand ARG form a certain interaction with water and improve the water retention of the gel.

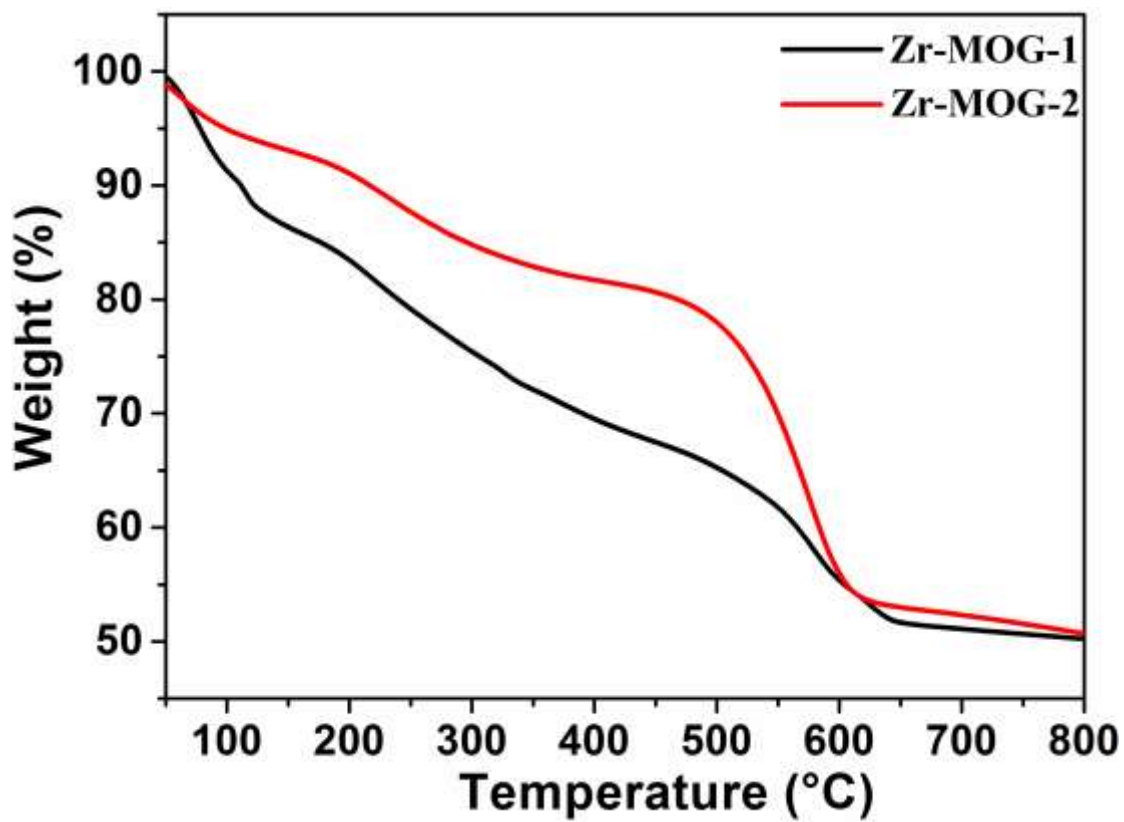


Fig. S6 TGA curves of Zr-MOG-1 xerogel and Zr-MOG-2 xerogel.

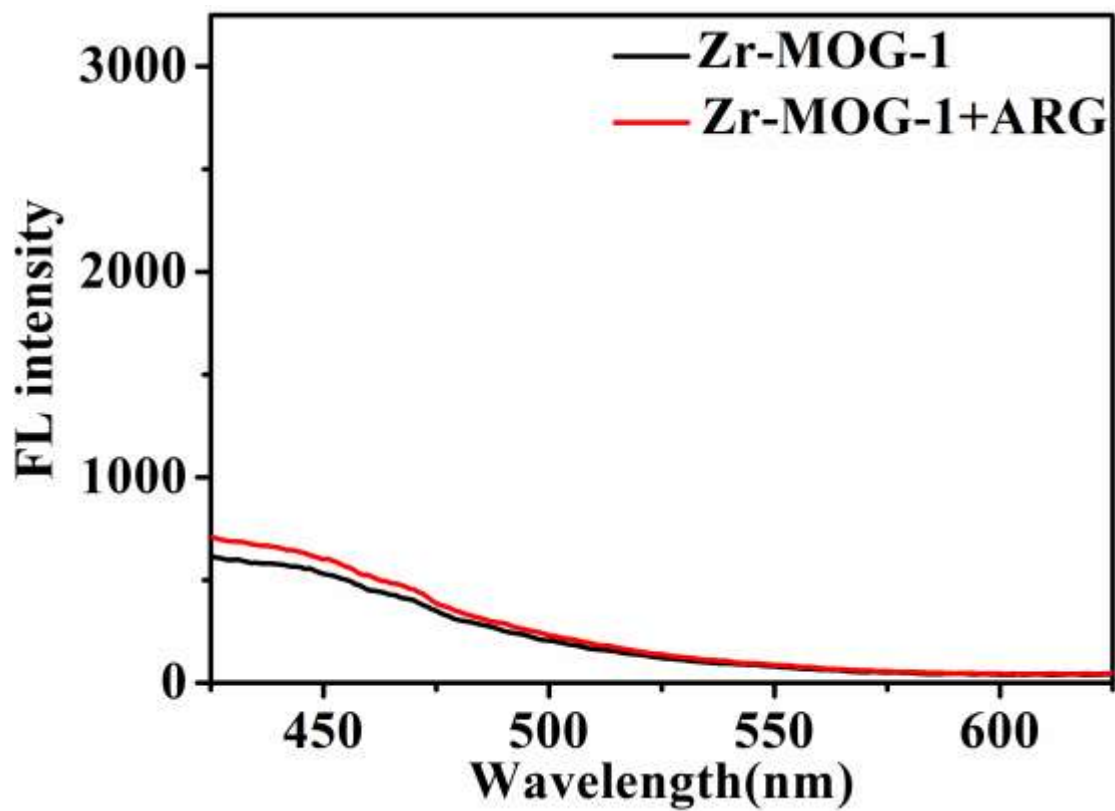


Fig. S7 Fluorescence emission spectra of Zr-MOG-1 and Zr-MOG-1 with ARG at 370 nm.

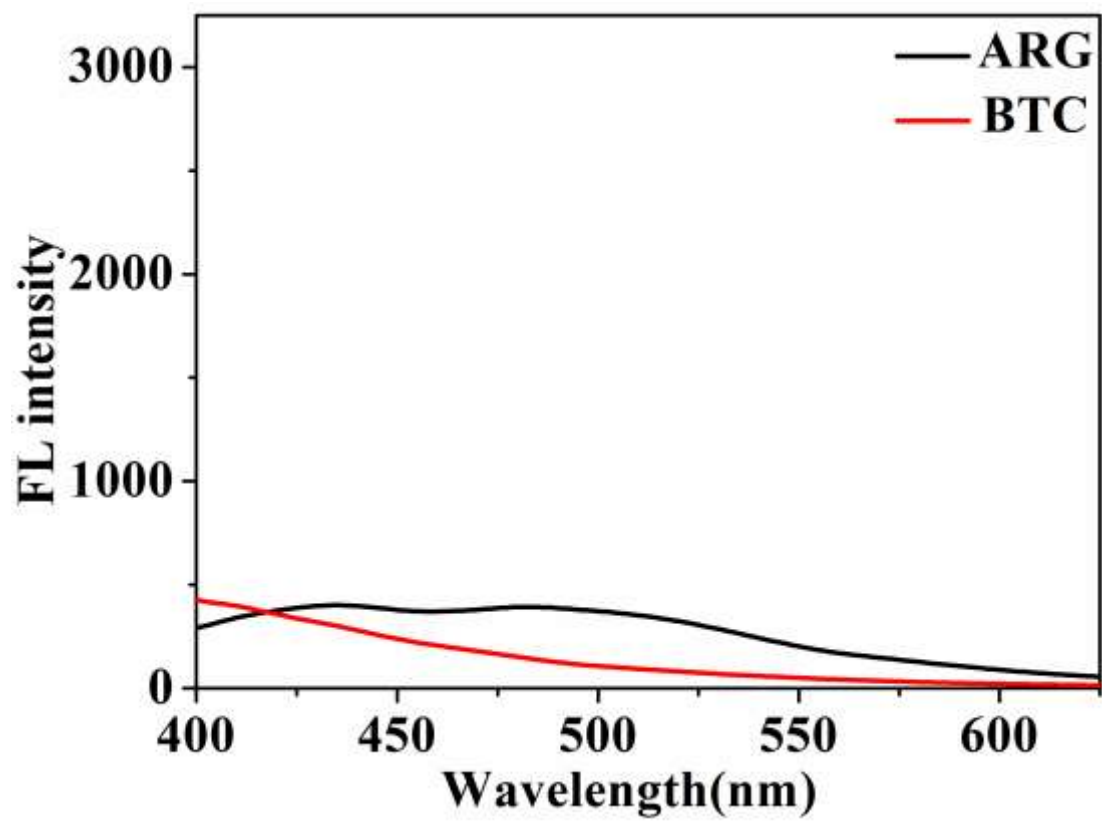


Fig. S8 Fluorescence emission spectra of BTC and ARG at 370 nm.

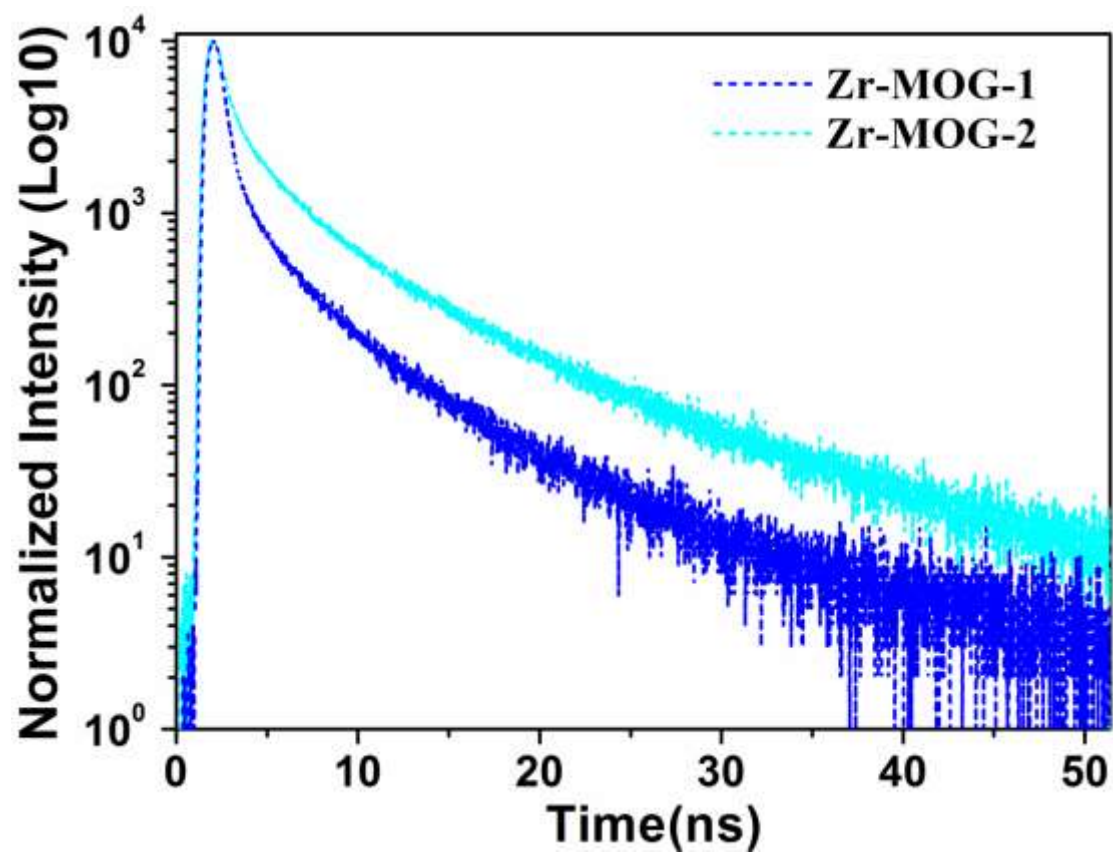


Fig. S9 Fluorescence lifetime spectra of **Zr-MOG-1** and **Zr-MOG-2**.

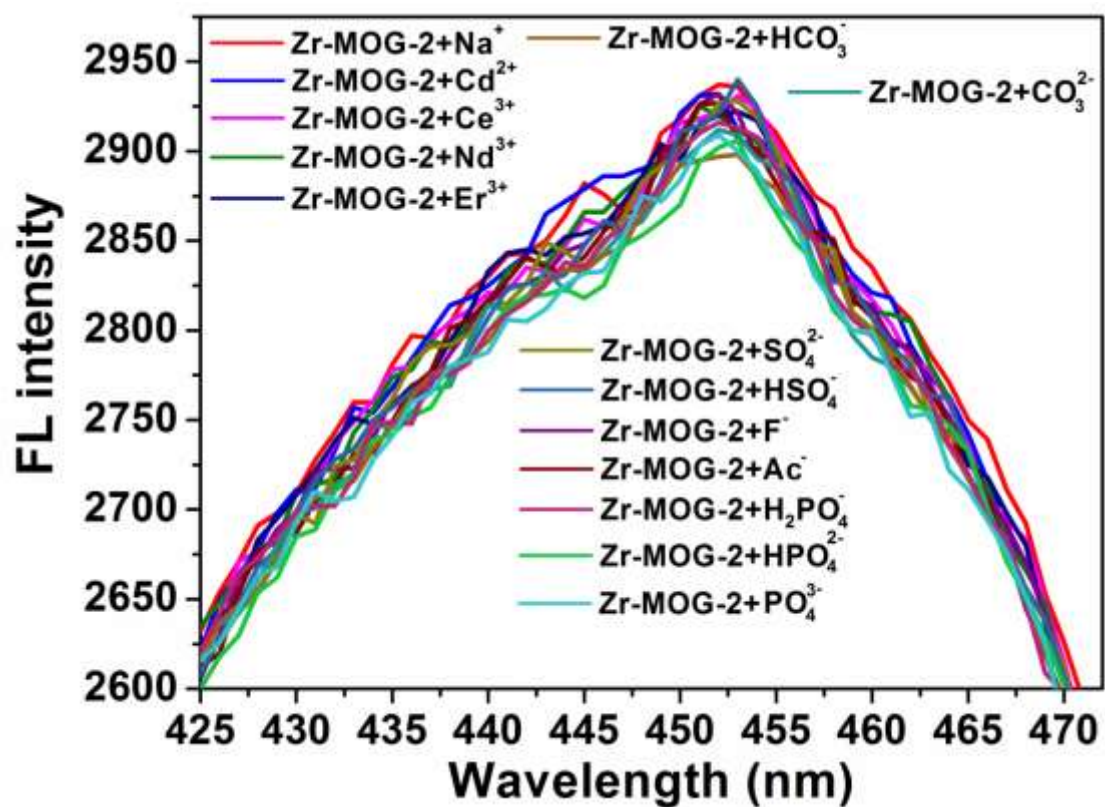


Fig. S10 Local fluorescence spectrum when **Zr-MOG-2** coexists with different single ion.

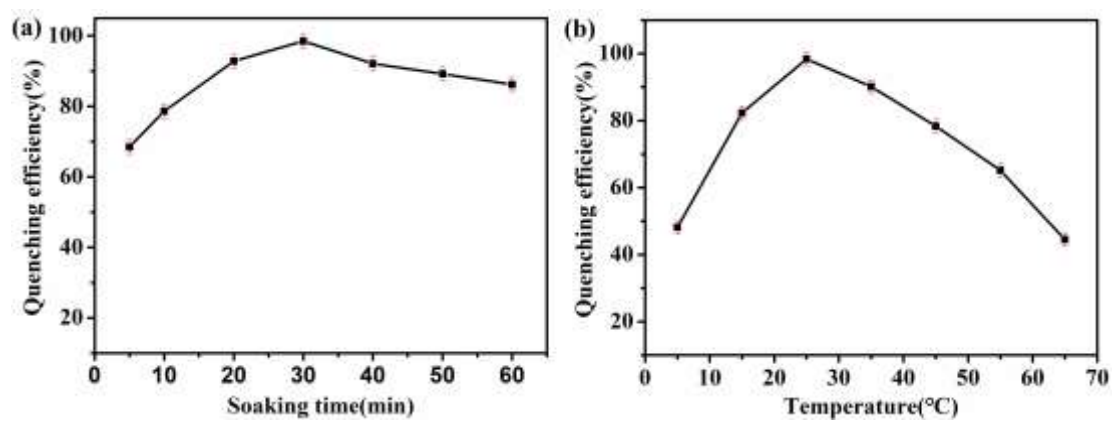


Figure S11 The effect of soaking time (a) and temperature (b) on the fluorescence quenching efficiency of **Zr-MOG-2**.

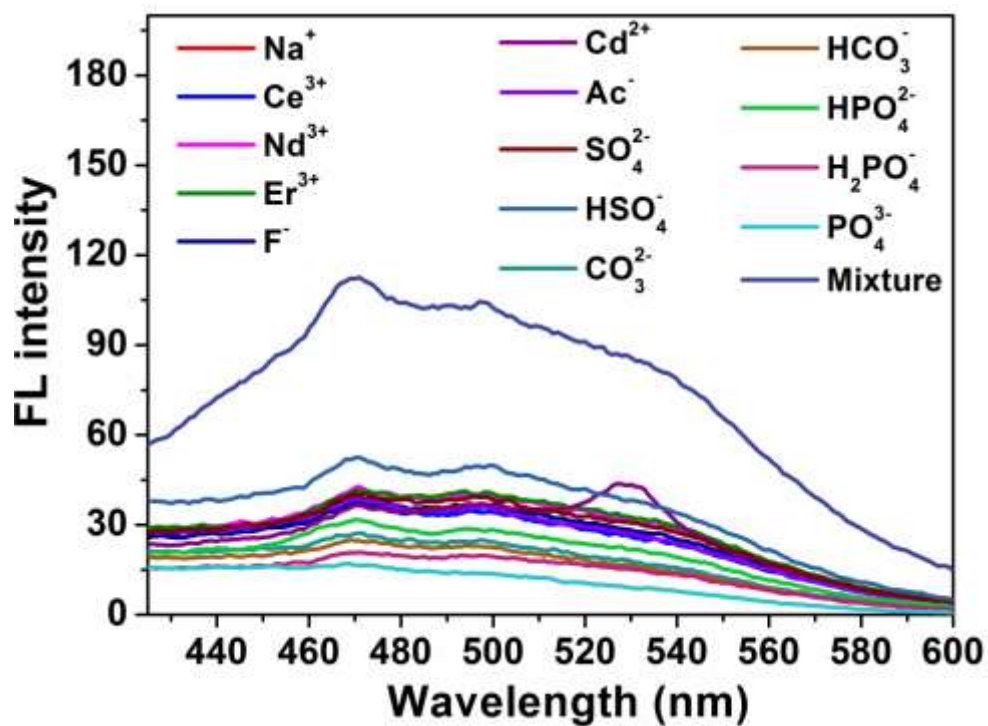


Fig. S12 Selectively optimized local spectra of **Zr-MOG-2** coexist with  $\text{CrO}_4^{2-}$  in the presence of other ions.

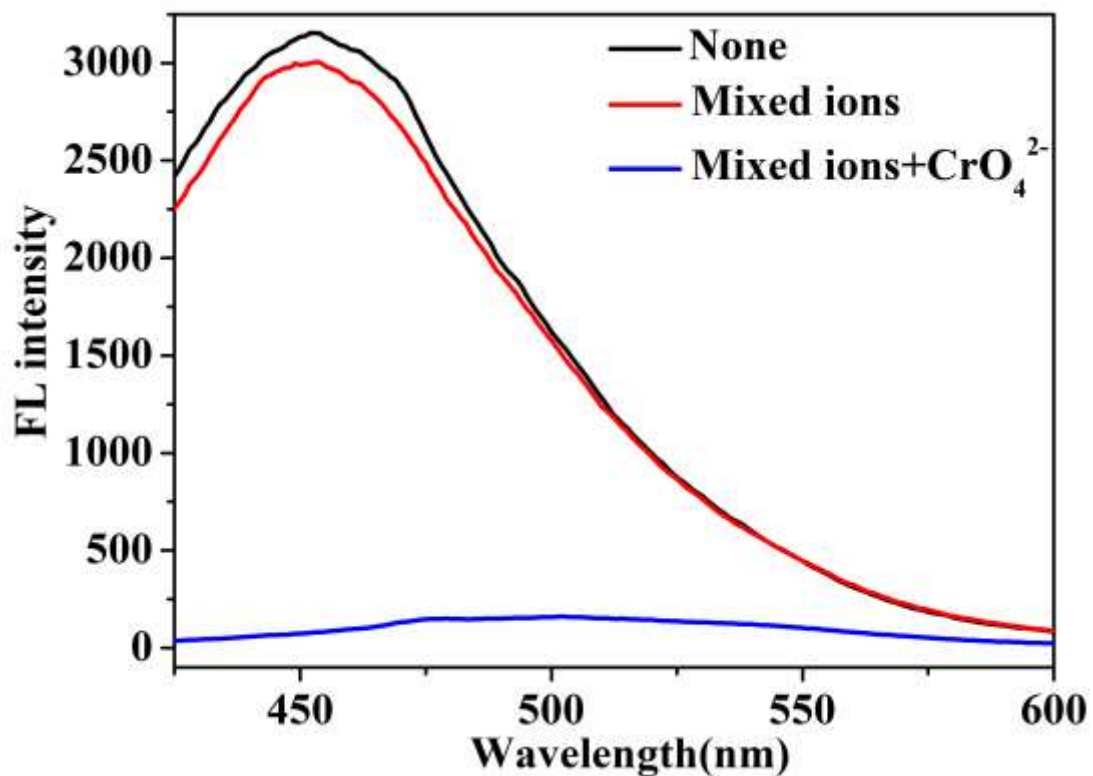


Fig. S13 Fluorescence emission spectra of **Zr-MOG-2** in the mixed ions solution with or without  $\text{CrO}_4^{2-}$  (0.1mM). Mixed ions:  $\text{Cd}^{2+}$ ,  $\text{Na}^+$ ,  $\text{Ce}^{3+}$ ,  $\text{Nd}^{3+}$ ,  $\text{Er}^{3+}$ ,  $\text{F}^-$ ,  $\text{Ac}^-$ ,  $\text{SO}_4^{2-}$ ,  $\text{HSO}_4^-$ ,  $\text{CO}_3^{2-}$ ,  $\text{HCO}_3^-$ ,  $\text{H}_2\text{PO}_4^-$ ,  $\text{HPO}_4^{2-}$  and  $\text{PO}_4^{3-}$  (0.1mM each)

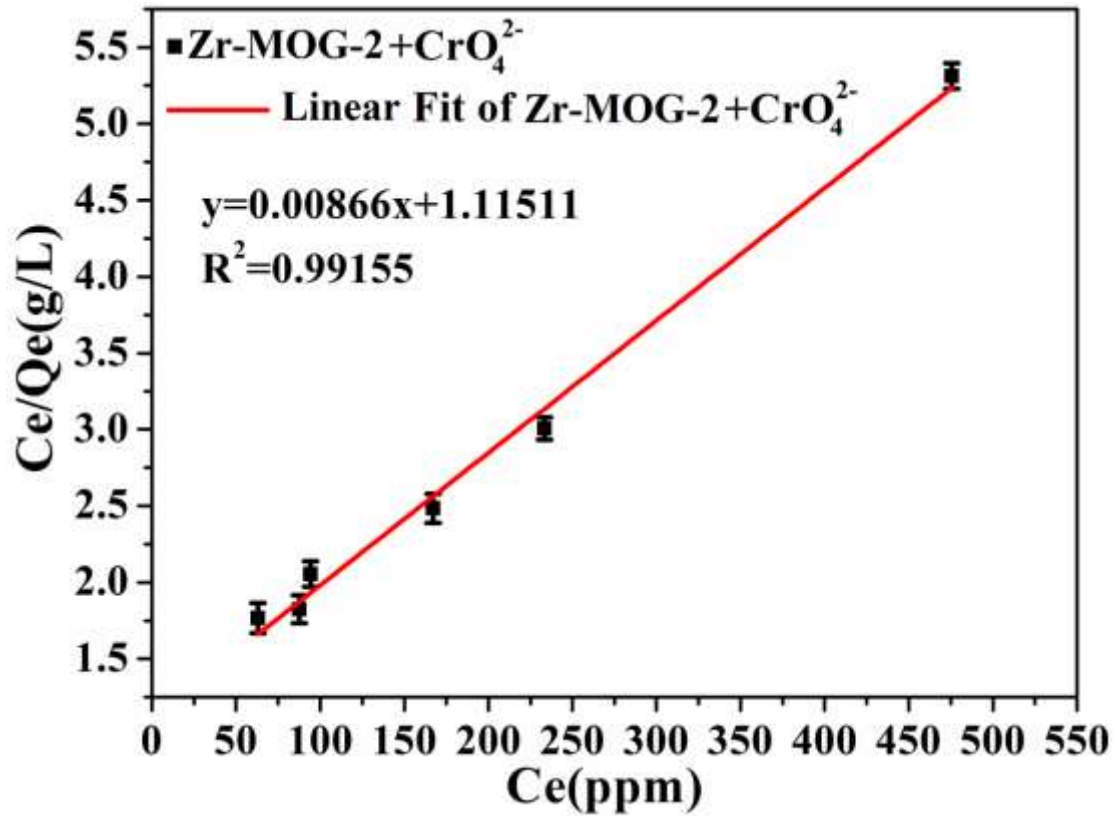


Fig. S14 Langmuir model fitting for the adsorption of  $\text{CrO}_4^{2-}$  by Zr-MOG-2 xerogel. The Langmuir model is as follows:

$$\frac{C_e}{Q_e} = \frac{C_e}{q_m} + \frac{1}{q_m K_L}$$

Where  $Q_e$  is the amount of  $\text{CrO}_4^{2-}$  adsorbed on the adsorbent at equilibrium;  $C_e$  represents the equilibrium concentration of  $\text{CrO}_4^{2-}$ ;  $q_m$  is the maximum adsorption capacity;  $K_L$  is the Langmuir constant.

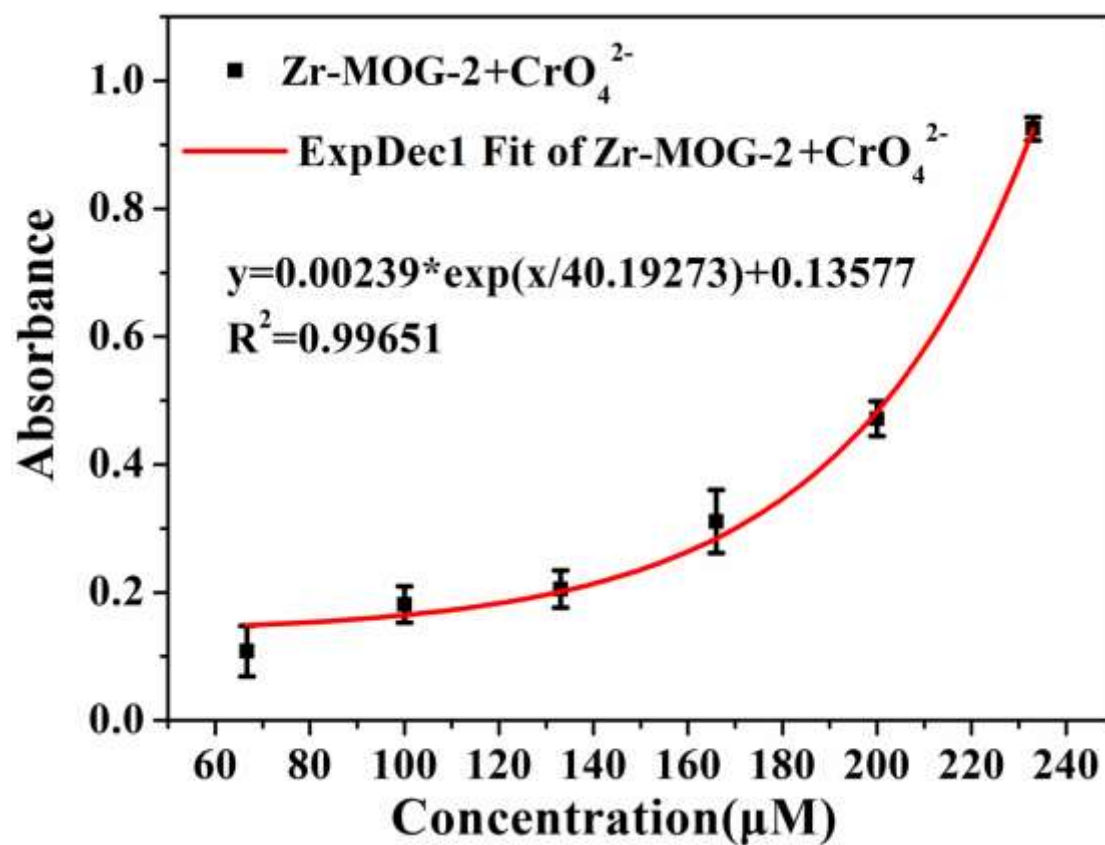


Fig. S15 The nonlinear fit curve of Zr-MOG-2 xerogel in a wide concentration of CrO<sub>4</sub><sup>2-</sup> aqueous solution.

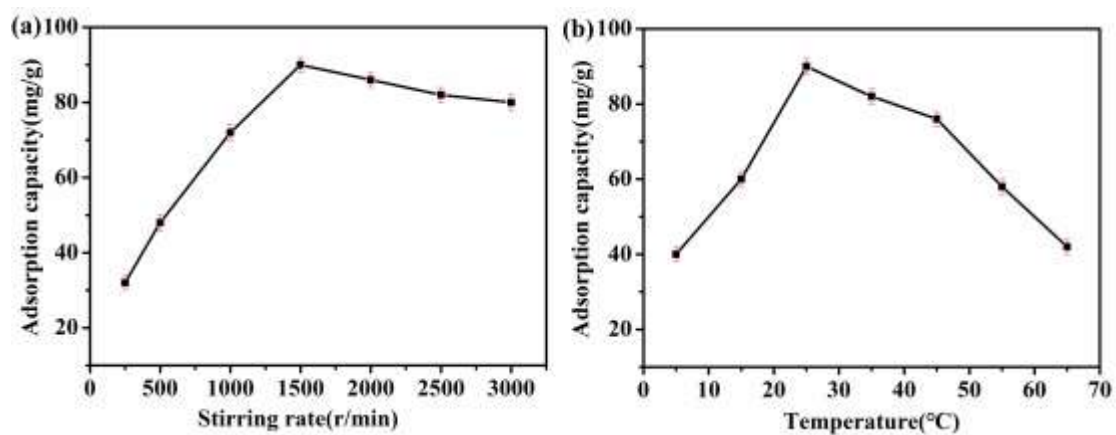


Fig. S16 Effects of (a) Stirring rate and (b) Temperature on the adsorption capacity of **Zr-MOG-2** xerogel adsorpt  $\text{CrO}_4^{2-}$ .

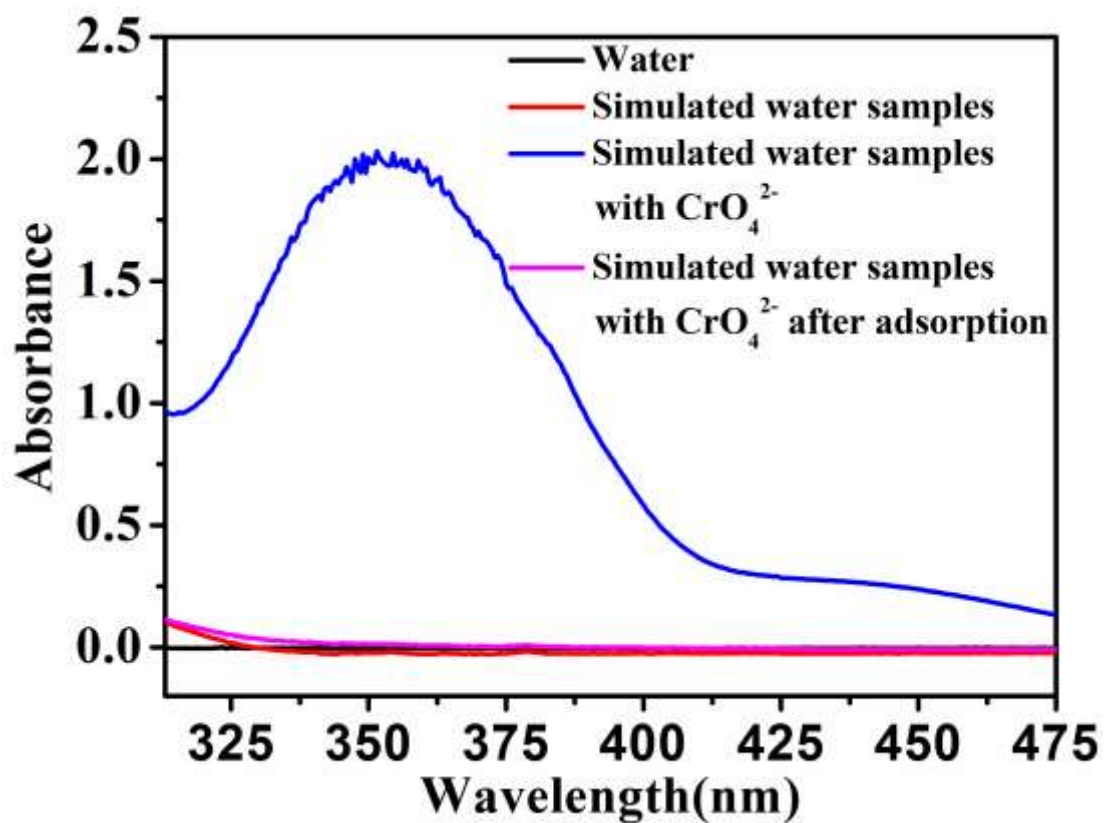


Fig. S17 UV-vis spectra of the simulated water samples with or without CrO<sub>4</sub><sup>2-</sup> before and after adsorption with Zr-MOG-2 xerogel.

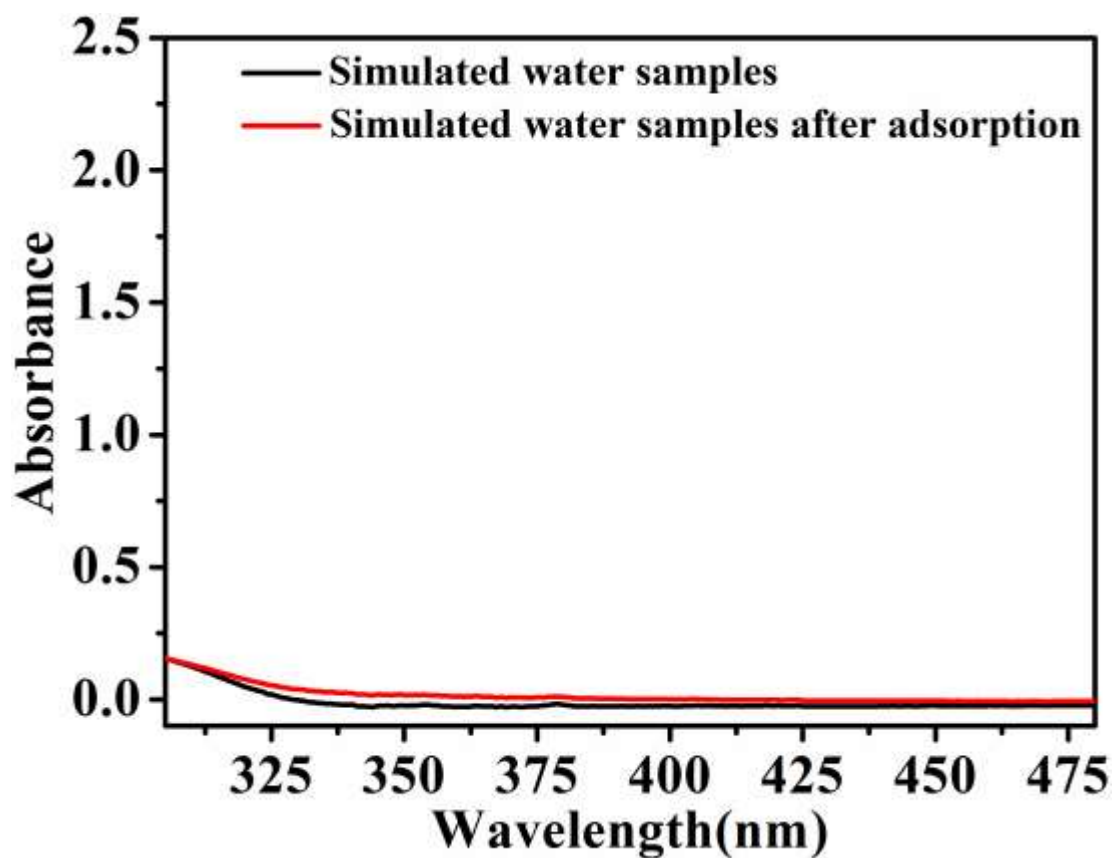


Fig. S18 UV-vis spectra of the simulated water samples before and after adsorption the removal process with Zr-MOG-2 xerogel.

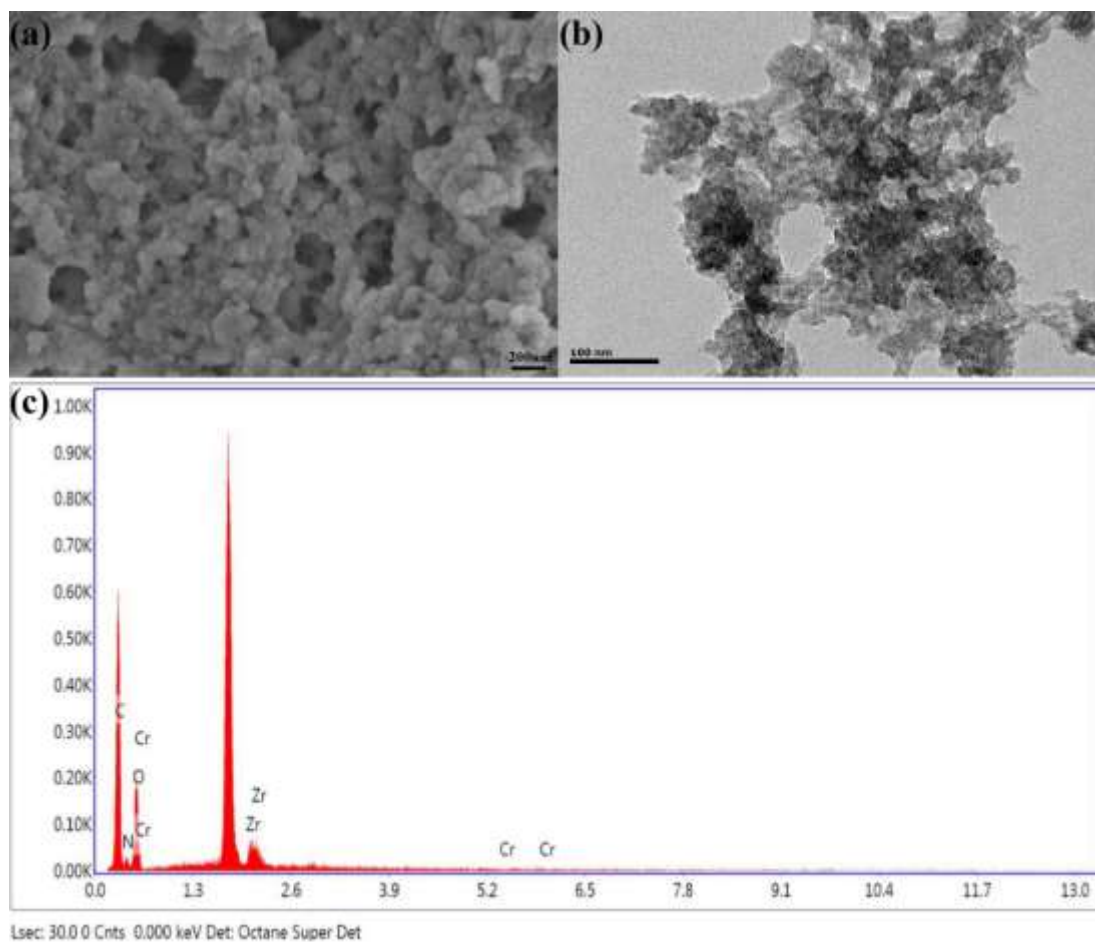


Fig. S19 SEM (a), TEM (b) and EDX (c) images of **Zr-MOG-2** xerogel after adsorption in simulated water samples with  $\text{CrO}_4^{2-}$ .

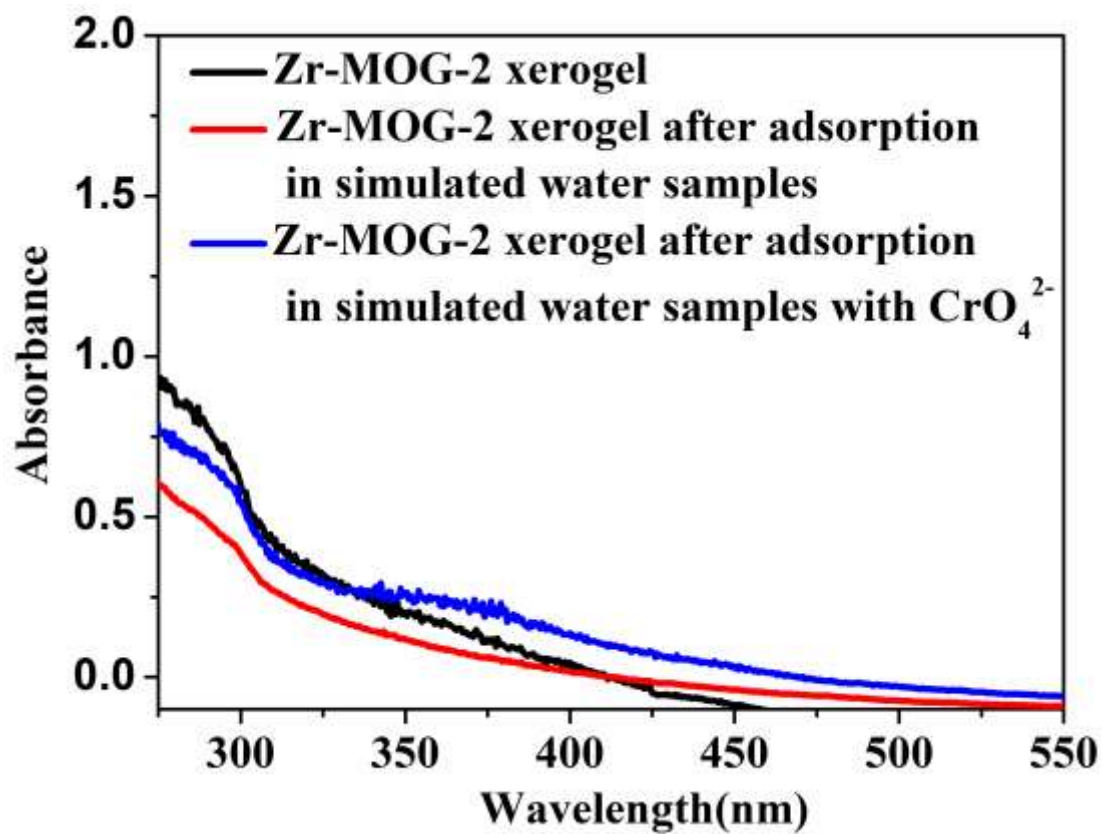


Fig. S20 UV-vis spectra of **Zr-MOG-2** xerogel, **Zr-MOG-2** xerogel after adsorption in simulated water samples and **Zr-MOG-2** xerogel after adsorption in simulated water samples with CrO<sub>4</sub><sup>2-</sup>.

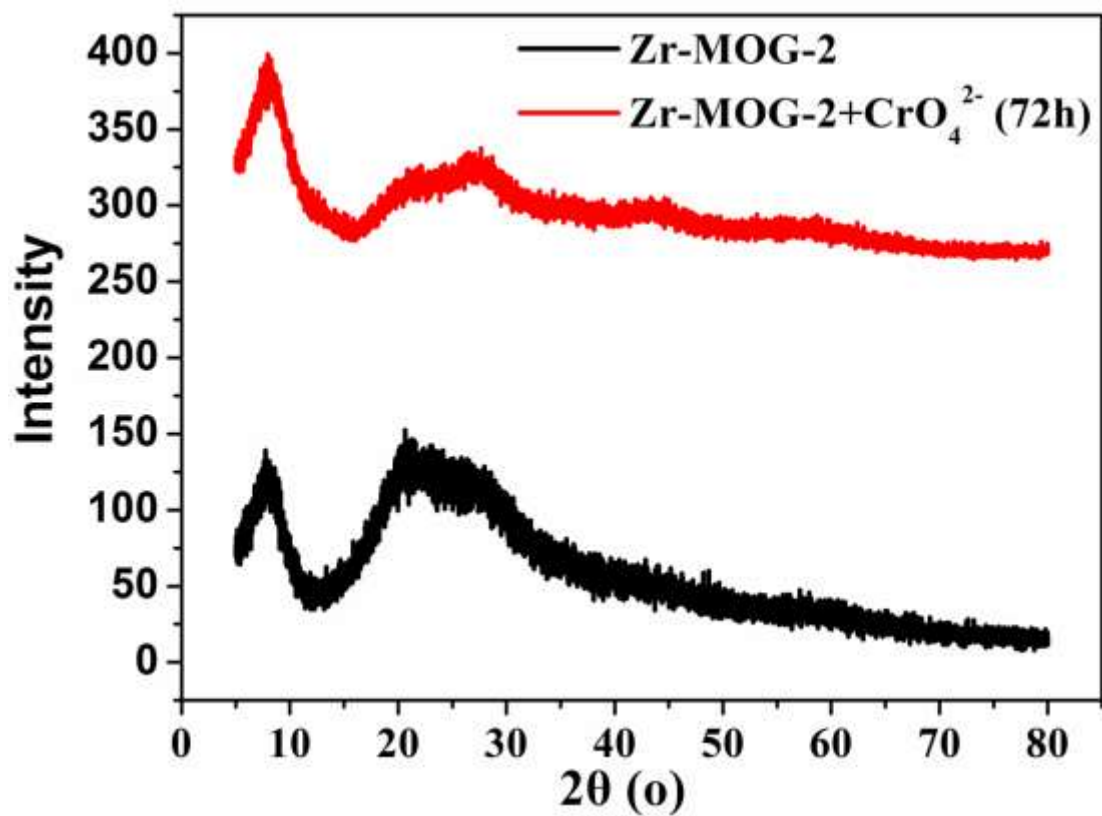


Fig. S21 XRD pattern of **Zr-MOG-2** xerogel after adsorption of CrO<sub>4</sub><sup>2-</sup>.

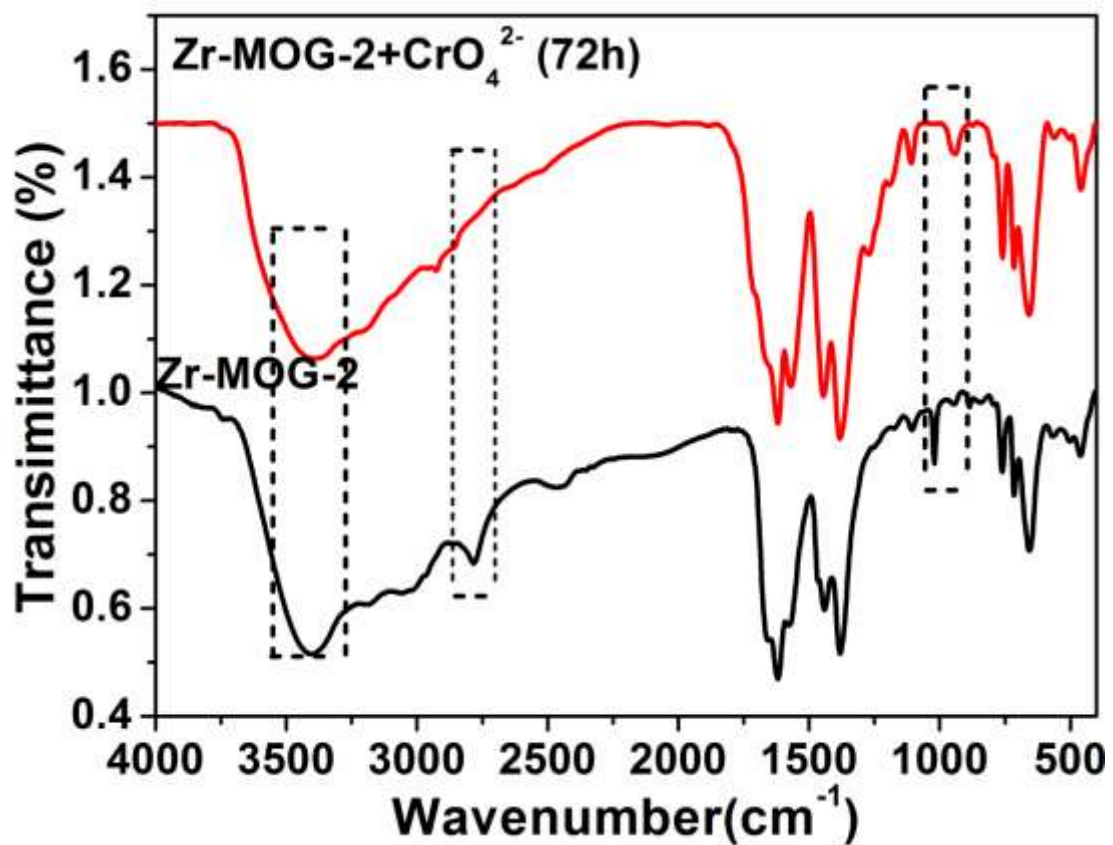


Fig. S22 FTIR spectrum of Zr-MOG-2 xerogel after adsorption of  $\text{CrO}_4^{2-}$ .

Table S1. Elemental analyses for **Zr-MOG-1** and **Zr-MOG-2**.

| <b>Materials</b> | <b>Element content (%)</b> |          |          |
|------------------|----------------------------|----------|----------|
|                  | <b>C</b>                   | <b>H</b> | <b>N</b> |
| <b>Zr-MOG-1</b>  | 39.87                      | 5.351    | 0.775    |
| <b>Zr-MOG-2</b>  | 29.22                      | 4.285    | 5.299    |

Table S2 The assay compared with reference for detection of  $\text{CrO}_4^{2-}$ .

| Materials used  | Analytical method          | Linear range (mM)                             | LOD (ppb)         | Reference |
|---|----------------------------|---|-------------------|-----------|
| $\{\text{[Zn(L)]}\cdot\text{CH}_3\text{CN}\}_n$   | Fluorescence               | 0-1   | $4.37\times 10^4$ | 1         |
| $\{\text{[Cd(CIP)}_2(\text{H}_2\text{O})_2]_n\cdot 2.5\text{H}_2\text{O}\}$   | Fluorescence               | $0-6.5\times 10^2$                            | $4.6\times 10^5$  | 2         |
| $[\text{Zn}_3(\text{DDB})(\text{DPE})]\cdot\text{H}_2\text{O}$  | Fluorescence               | 0-0.1   | 75                | 3         |
| $[\text{Zn}_2(\text{TPOM})(\text{ND C})_2]\cdot 3.5\text{H}_2\text{O}$  | Fluorescence               | $0-1.6\times 10^{-3}$                         | $5.13\times 10^2$ | 4         |
| $[\text{Zn}_2(\text{TPOM})(\text{NH}_2\text{-BDC})_2]\cdot 4\text{H}_2\text{O}$   | Fluorescence               | 0-0.1   | $5.58\times 10^2$ | 5         |
| $\{\text{[Cd(bimb)Cl}_2]\cdot 1.5\text{H}_2\text{O}\}_n$  | Fluorescence               | 0-0.03  | $2.17\times 10^3$ | 6         |
| $\{\text{[Cd}_{1.5}(\text{bbib})_{2.5}\text{Cl}_2]\cdot 3\text{H}_2\text{O}\cdot \text{NO}_3\}_n$   | Fluorescence               | 0-0.035                                       | $3.30\times 10^3$ | 6         |
| USTC-5  | Fluorescence               | 0-1   | $2.21\times 10^3$ | 7         |
| $[[\text{Zn}_3(\mu_4\text{-cpboda})_2(\mu_2\text{-H}_2\text{O})_2(\text{DMF})_2(\text{H}_2\text{O})_2]\cdot 3\text{DMF}\cdot 3\text{HCOOH}\cdot 3\text{H}_2\text{O}]_n$ | Fluorescence               | 0-0.055                                       | 600               | 8         |
| 1 $\beta$ -DMAc   | Fluorescence               | 0-0.14  | $4.44\times 10^2$ | 9         |
| <b>Zr-MOG-2</b>   | Fluorescence<br>"turn off" | $0.5\times 10^{-3}$ -<br>$10.2\times 10^{-3}$ | 5.2               | This work |

Table S3 Fluorescence lifetime of **Zr-MOG-2** treated with different concentrations of  $\text{CrO}_4^{2-}$ .

| Analyzed material  | Fluorescence lifetime ( $\tau$ , s) |
|--|-------------------------------------|
| <b>Zr-MOG-2</b>  | $2.23 \times 10^{-10}$              |
| <b>Zr-MOG-2</b> + $\text{CrO}_4^{2-}$ (6.7 $\mu\text{M}$ ) | $1.04 \times 10^{-10}$              |
| <b>Zr-MOG-2</b> + $\text{CrO}_4^{2-}$ (67 $\mu\text{M}$ )  | $9.75 \times 10^{-11}$              |
| <b>Zr-MOG-2</b> + $\text{CrO}_4^{2-}$ (670 $\mu\text{M}$ ) | $9.62 \times 10^{-11}$              |

Resonance energy transfer efficiency is calculated from following equation:

$$Q = \left(1 - \frac{\tau}{\tau_0}\right) \times 100\% \quad \text{S3}$$

where  $\tau$  is the fluorescence lifetime of the Zr-MOG-2 after treatment with different concentrations of  $\text{CrO}_4^{2-}$ ,  $\tau_0$  is the fluorescence lifetime of pure Zr-MOG-2.

Table S4 The adsorption compared with reference of  $\text{CrO}_4^{2-}$

| Adsorbent  | Qm (mg/g) | Reference |
|--|-----------|-----------|
| Magnetic biochar   | 77.5      | 10        |
| $\{[\text{Ag}_8(\text{tz})_6](\text{NO}_3)_2 \cdot 6\text{H}_2\text{O}\}_n$        | 37        | 11        |
| $[\text{Zn}_2(\text{TIPA})_2(\text{OH})(\text{NO}_3)_3] \cdot 5\text{H}_2\text{O}$ | 133.8     | 12        |
| UiO-66-me-PyDC   | 50.1      | 13        |
| $[\text{Co}_2(\text{btec})-(\text{bipy})(\text{DMF})_2]_n$                         | 30.68     | 14        |
| BiOBr  | 32.5      | 15        |
| <b>Zr-MOG-2</b> xerogel  | 90        | This work |

### Notes and references

1. J. Li, T. J. Chen, S. Han and L. F. Song, Four Zn(II)-organic frameworks as luminescent probe for highly selectivity detection of  $\text{Cr}^{\text{VI}}$  ions and antibiotics, *Journal of Solid State Chemistry*, 2019, **277**, 107-114.
2. X. Q. Wang, D. D. Feng, Y. D. Zhao, D. D. Fang, J. Tang, L. M. Fan and J. Yang, A multifunctional 1D Cd-based metal-organic complex for the highly luminescent sensitive detection of  $\text{Fe}^{3+}$ ,  $\text{CrO}_4^{2-}/\text{Cr}_2\text{O}_7^{2-}$ , and nitroaromatic explosives, *Journal of Solid State Chemistry*, 2019, **274**, 40-46.
3. X. Q. Wang, D. D. Feng, J. Tang, Y. D. Zhao, J. Li, J. Yang, C. K. Kim and F. Su, A water-stable zinc(ii)-organic framework as a multiresponsive luminescent sensor for toxic heavy metal cations,

- oxyanions and organochlorine pesticides in aqueous solution, *Dalton Transactions*, 2019, **48**, 16776-16785.
4. R. Lv, H. Li, J. Su, X. Fu, B. Yang, W. Gu and X. Liu, Zinc Metal-Organic Framework for Selective Detection and Differentiation of Fe(III) and Cr(VI) Ions in Aqueous Solution, *Inorganic Chemistry*, 2017, **56**, 12348-12356.
  5. R. Lv, J. Y. Wang, Y. P. Zhang, H. Li, L. Y. Yang, S. Y. Liao, W. Gu and X. Liu, An amino-decorated dual-functional metal-organic framework for highly selective sensing of Cr(III) and Cr(VI) ions and detection of nitroaromatic explosives, *Journal of Materials Chemistry A*, 2016, **4**, 15494-15500.
  6. Y. Qu, L. Gao and Y. Zhang, TWO 3D Cd (II) luminescent coordination polymers as highly selective and sensitive sensing for  $\text{Fe}^{3+}$  and  $\text{CrO}_4^{2-}/\text{Cr}_2\text{O}_7^{2-}$  ions in aqueous system, *Journal of Solid State Chemistry*, 2020, **292**, 121637.
  7. B. Li, Q. Yan and G. Yong, A new porous coordination polymer reveals selective sensing of  $\text{Fe}^{3+}$ ,  $\text{Cr}_2\text{O}_7^{2-}$ ,  $\text{CrO}_4^{2-}$ ,  $\text{MnO}_4^-$  and nitrobenzene, and stimuli-responsive luminescence color conversions, *Journal of Materials Chemistry C*, 2020, **8**, 11786-11795.
  8. D. Yang, L. Lu and M. Zhu, Structural diversity, magnetic properties, and luminescence sensing based Ni(II)/Zn(II) coordination polymers of the semirigid 3,3'-((5-carboxy-1,3-phenylene)bis(IJoxy))dibenzate ligand, *CrystEngComm*, 2020, **22**, 5207-5217.
  9. Y. Huang, P. Chuang, and J. Wu, Solvent-Induced Controllable Supramolecular Isomerism: Phase Transformation,  $\text{CO}_2$  Adsorption, and Fluorescence Sensing toward  $\text{CrO}_4^{2-}$ ,  $\text{Cr}_2\text{O}_7^{2-}$ ,  $\text{MnO}_4^-$ , and  $\text{Fe}^{3+}$ , *Inorganic Chemistry*, 2020, **59**, 9095–9107.
  10. Y. Han, X. Cao, X. Ouyang, S. P. Sohi and J. Chen, Adsorption kinetics of magnetic biochar derived from peanut hull on removal of Cr (VI) from aqueous solution: Effects of production conditions and particle size, *Chemosphere*, 2016, **145**, 336-341.
  11. L. L. Li, X. Q. Feng, R. P. Han, S. Q. Zang and G. Yang, Cr(VI) removal via anion exchange on a silver-triazolate MOF, *Journal of Hazardous Materials*, 2017, **321**, 622-628.
  12. H. R. Fu, N. Wang, J. H. Qin, M. L. Han, L. F. Ma and F. Wang, Spatial confinement of a cationic MOF: a SC-SC approach for high capacity Cr(vi)-oxyanion capture in aqueous solution, *Chemical Communications*, 2018, **54**, 11645-11648.
  13. C. Jiang, R. Sun, Z. Du, V. Singh and S. Chen, A cationic Zr-based

- metal organic framework with enhanced acidic resistance for selective and efficient removal of  $\text{CrO}_4^{2-}$ , *New Journal of Chemistry*, 2020, **44**, 12646.
14. K. Zuo, X. Huang, X. Liu, E. M. G. Garcia, J. Kim, A. Jain, L. Chen, P. Liang, A. Zepeda, R. Verduzco, J. Lou, and Q. Li, A Hybrid Metal-Organic Framework-Reduced Graphene Oxide Nanomaterial for Selective Removal of Chromate from Water in an Electrochemical Process, *Environmental Science & Technology*, 2020, **54**, 13322-13332.
  15. L. Jia, W. Zhou, X. Huang, Y. Zhang, Q. Zhang, X. Tan and T. Yu, Enhanced adsorption of Cr(VI) on BiOBr under alkaline conditions: interlayer anion exchange, *Environmental Science Nano*, 2019, **6**, 3601–3610